Initial experiments on the shock-ignition inertial confinement fusion concept[a]

W. Theobald,[1,b] R. Betti,[1,2,3] C. Stoeckl,[1] K. S. Anderson,[1] J. A. Delettrez,[1] V. Yu. Glebov,[1]
V. N. Goncharov,[1,2] F. J. Marshall,[1] D. N. Maywar,[1] R. L. McCrory,[1,2,3]
D. D. Meyerhofer,[1,2,3] P. B. Radha,[1] T. C. Sangster,[1] W. Seka,[1] D. Shvarts,[1]
V. A. Smalyuk,[1] A. A. Solodov,[1] B. Yaakobi,[1] C. D. Zhou,[1] J. A. Frenje,[4] C. K. Li,[4]
F. H. Séguin,[4] R. D. Petrasso,[4] and L. J. Perkins[5]

[1]*Fusion Science Center and Laboratory for Laser Energetics, University of Rochester, Rochester,
New York 14623, USA*
[2]*Department of Mechanical Engineering, University of Rochester, Rochester, New York 14623, USA*
[3]*Department of Physics and Astronomy, University of Rochester, Rochester, New York 14623, USA*
[4]*Massachusetts Institute of Technology, Cambridge, Massachusetts 02139, USA*
[5]*Lawrence Livermore National Laboratory, Livermore, California 94550, USA*

Shock ignition is a two-step inertial confinement fusion concept where a strong shock wave is launched at the end of the laser pulse to ignite the compressed core of a low-velocity implosion. Initial shock-ignition technique experiments were performed at the OMEGA Laser Facility [T. R. Boehly *et al.*, Opt. Commun. **133**, 495 (1997)] using 40-μm-thick, 0.9-mm-diam, warm surrogate plastic shells filled with deuterium gas. The experiments showed a significant improvement in the performance of low-adiabat, low-velocity implosions compared to conventional "hot-spot" implosions. High areal densities with average values exceeding $\sim$0.2 g/cm^2 and peak areal densities above 0.3 g/cm^2 were measured, which is in good agreement with one-dimensional hydrodynamical simulation predictions. Shock-ignition technique implosions with cryogenic deuterium and deuterium-tritium ice shells produced areal densities close to the 1D prediction and achieved up to 12% of the predicted 1D fusion yield. © *2008 American Institute of Physics.*
[DOI: 10.1063/1.2885197]

I. INTRODUCTION

Shock ignition is a concept for direct-drive laser inertial confinement fusion (ICF) (Refs. 1–3) that was recently proposed by Betti *et al.*[4,5] It promises to achieve ignition with $\sim$3-times-lower driver energy than the conventional isobaric hot-spot ignition concept.[6] The fuel is assembled to a high areal density (ρR) on a low adiabat (α) with a subignition implosion velocity using shaped nanosecond laser pulses. The adiabat[3] is defined as the ratio of the plasma pressure to the Fermi pressure of a degenerate electron gas and is typically $\alpha \sim 1$–2. Because of the low implosion velocity, the temperature of the central hot spot is too low for conventional ignition to occur. Then a strong shock wave launched at the end of the laser pulse with an intensity spike hits the compressed core, further compresses the hot spot, and triggers ignition. The resulting burn wave ignites the entire dense core, producing high yields due to the large areal densities. Similar to fast ignition[7] and impact ignition,[8] the fuel assembly and ignition are separated and the energy gain (G) scales as $G \sim \theta/v_i^{1.25}$ (Ref. 9), where θ is the burn up fraction that increases with ρR (Ref. 2) and v_i denotes the implosion velocity. A low-implosion velocity and high ρR are advantageous to producing the highest ICF gains.[4] The peak areal density is approximately independent of the shell-implosion velocity and depends on the in-flight adiabat according to

$(\rho R)_{max} \sim \alpha^{-0.6}$ (Ref. 4), favoring an adiabat as low as achievable. Low-velocity, high-ρR, $\alpha \approx 1.5$ implosions have recently demonstrated experimentally a neutron-averaged areal density of 0.13 g/cm^2 and peak ρR of $\sim$0.24 g/cm^2 (Ref. 10). In fast ignition, the implosion laser facility must be combined with a high-intensity, short-pulse, multipetawatt-ignitor laser facility delivering a particle beam for ignition. Shock ignition makes use of the pulse-shaping capabilities of the implosion laser facility, significantly relaxing the technical constraints on the concept.

The strong shock wave that triggers ignition is achieved by adding a sharp intensity spike at the end of the main drive pulse.[4] The laser power must rise to several hundred terawatts in a few hundred picoseconds to drive the ignitor shock. The spike pulse is timed so that the shock wave meets with the return shock driven by the rising hot-spot pressure during the deceleration phase in the shell close to the cold fuel/hot spot interface. The colliding shocks generate two new shock waves with one propagating inward, leading to further compression of the hot spot and a peaked pressure profile with its maximum in the center. The resulting fuel assembly is nonisobaric with a hot-spot pressure greater than the surrounding dense fuel pressure[4] and, to achieve ignition, requires a lower energy than the conventional isobaric hot-spot ignition.[4,5] The required driver energy is lowered roughly by the factor $(p_{hs}/p_{iso})^{2.5}$ (Ref. 5), where p_{hs} is the nonisobaric hot-spot pressure and p_{iso} is the isobaric pressure. A pressure ratio of $\sim$1.6 results in a three-times-lower

ignition energy. This mechanism is very effective in thick-shell implosions, where the ignitor shock wave significantly increases its strength as it propagates through the converging shell. Massive shell implosions have good hydrodynamic-stability properties during the acceleration phase because of low acceleration and small in-flight aspect ratio (IFAR). The number of *e*-foldings of Rayleigh–Taylor (RT) instability growth for the most-dangerous modes with wave numbers about equal to the inverse in-flight target thickness is roughly proportional to the square root of IFAR.[3] Low IFAR implosions are not significantly affected by RT instability.

This paper describes initial implosion experiments of the shock-ignition concept that were performed on the OMEGA Laser System[11] using warm plastic surrogate shells and cryogenic shell targets. The power of the OMEGA laser is limited to about 20 TW, thus preventing the investigation of the shock-ignition scheme in ignition-relevant regimes (requiring more than 300 TW). Nevertheless, by lowering the power during the assembly pulse to about 7 TW, a late shock can be launched by a fast rise to about 18 TW. Such OMEGA experiments are used to study important features of the shock-ignition scheme such as hydrodynamic stability, shell compression, and hot-spot compression induced by the late shock. One of the most important aspects to be investigated is the uniformity of the shock-induced hot-spot compression. Since the ignitor shock is launched late in the pulse, its uniformity might be compromised by the large amplitude modulations of the ablation front. The ignitor shock could transfer such perturbations from the ablation front to the hot spot, thus reducing the uniformity of the compression and possibly quenching the thermonuclear burn. By comparing the implosion performance with and without a shock, we infer the relative effectiveness of the shock compression and hot-spot heating. The low-mode uniformity of the compression is assessed by measuring the modulation in the areal density and by the magnitude of the neutron yield with respect to the calculated 1D yield. Varying the timing of the peaks in the laser pulse shape optimizes the timing of the shock waves and the implosion performance. Plastic-shell implosions study how fuel-shell mixing affects the yield performance for shock-ignition pulse shapes, compared to standard low-adiabat picket-pulse capsule implosions.[10] Significantly improved performance using shock-ignition-type pulse shapes has been observed, leading to peak ρR exceeding ~ 0.3 g/cm^2. The following four sections present the target types, the laser pulse shapes, and diagnostics (Sec. II); fusion-reaction yield measurements of plastic-shell implosions (Sec. III); areal-density analysis of plastic-shell implosions (Sec. IV); and initial spike pulse cryogenic-shell implosions (Sec. V). A summary and conclusions are presented in Sec. VI.

II. TARGETS, LASER PULSE SHAPES, AND DIAGNOSTICS

Figure 1 shows the targets that were used in the experiments: (a) 40-μm-thick, 430-μm-outer-radius, plastic (CH) shells coated outside with a 0.1-μm layer of aluminum and filled with D$_2$ gas with pressures ranging from 4 to 45 atm
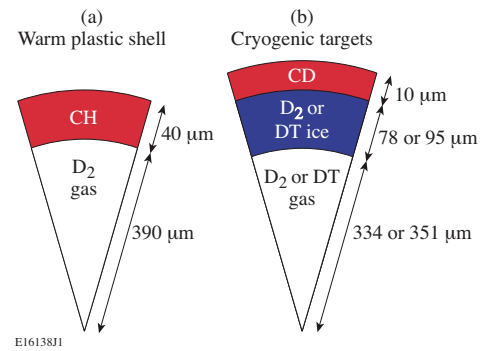

FIG. 1. (Color online) Targets that were used to test shock-ignition pulse-shape implosions on the OMEGA Laser Facility.

and (b) cryogenic targets comprising a 10-μm-thick, strong deuterated plastic shell and frozen layers of 95-μm-deuterium (D$_2$) and 78-μm-deuterium-tritium (DT) ice, respectively. Details of the direct-drive cryogenic-target program can be found in Refs. 12–14.

The capsules were imploded by relaxation adiabat shaping[9] laser pulses of $\sim$16 to 20-kJ UV laser energy. The 351-nm-wavelength laser light was smoothed with polarization smoothing[15] and distributed phase plates,[16] and in some shots the laser beam was smoothed with 1-THz-bandwidth, 2D smoothing by spectral dispersion (SSD).[17] Typical experimental pulse shapes with and without spike for warm plastic targets and $\alpha \sim 1.5$ are compared in Fig. 2. The shaped pulses comprise an 80-ps full width at half maximum (FWHM) Gaussian prepulse ("picket pulse") and a subsequent shaped main-drive portion consisting of an $\sim$1-TW foot power and a moderate $\sim$6 to 8-TW plateau; the solid curve comprises a high-intensity spike portion ("spike pulse") with a peak power of about $\sim$17 TW. The corresponding nominal laser intensity in the spike portion exceeds 7×10^{14} W/cm^2. The nominal laser intensity refers to the initial target size, while the actual intensity at the critical-density surface at the pulse end is a factor of $\sim$2 higher due to compression. A similar pulse shape without spike but the same laser energy is shown by the dashed curve. The pulse shapes are very similar in the first nanosecond, including the picket intensity, the picket timing, and the foot of the main
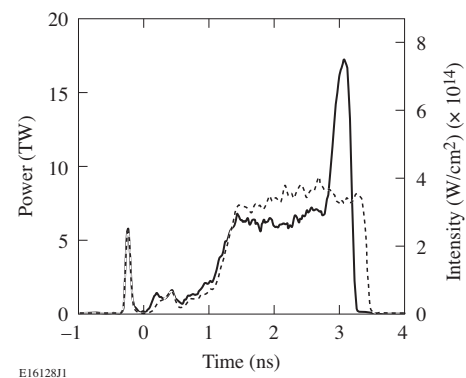

FIG. 2. Pulse shapes with (solid curve, 46078) and without spike (dashed, 46073), no SSD. The laser energies were 18.6 kJ (46078) and 19.4 kJ (46073), respectively. The onset of the spike pulse was at 2.8 ns.
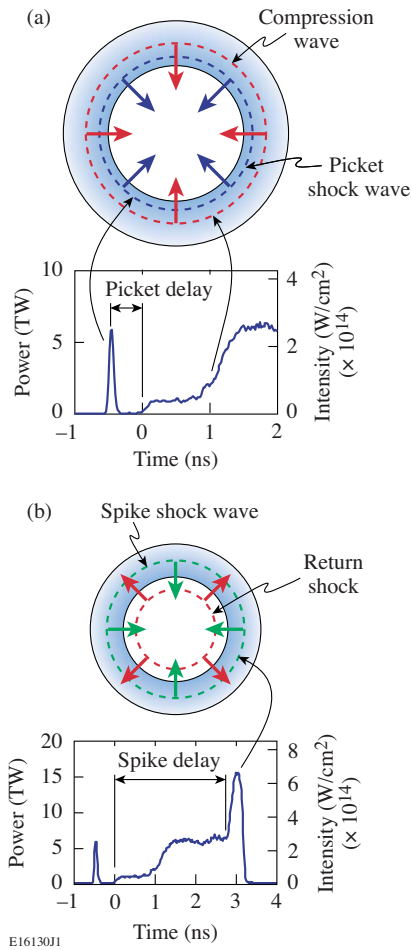
FIG. 3. (Color online) Schematic of the timing of the various shock waves generated by the picket pulse, the drive pulse, and the high-intensity spike pulse. SW, shock wave by picket pulse; CW, compression wave; SSW, spike shock wave.

drive pulse. The no-spike shape reaches a slightly higher power in the plateau. The energy difference in the plateau is transferred to form the spike (solid curve). Zero time marks the onset of the foot of the main drive laser pulse. The picket pulse in front of the foot of the main pulse launches a shock wave that sets the adiabat of the implosion and generates a shaped-adiabat profile within the shell that is monotonically decreasing from the outer (ablation) surface toward the inner shell surface (see Fig. 2 in Ref. 10). The use of adiabat-shaping pulses in the context of fast-ignition implosions was suggested in Ref. 9. The relaxation technique[18,19] for adiabat shaping simplifies the laser pulse by lowering the contrast ratio between the peak laser power and the power in the foot of the main pulse. It also improves the hydrodynamic stability of the implosion by decreasing the in-flight aspect ratio and increasing the ablation velocity.

Figure 3 shows a schematic of the timing of the various shock waves in a warm surrogate shock-ignition implosion. The picket pulse that is optimally timed with respect to the main drive pulse launches a shock wave (SW) and sets the adiabat of the implosion. The slowly rising part of the main drive launches a compression wave (CW) steepening up while propagating through the shell and then overtakes the

SW just before shock breakout at the inner interface. A sharp rise in intensity at the end (spike pulse) generates a "spike shock wave" (SSW) that must be properly timed to meet the return shock in the inner region of the cold shell material. The colliding shocks then generate the shock wave that travels back to the capsule center. In the experiments, the implosion was optimized by measuring the fuel assembly performance as a function of the timing of the picket and spike pulses. The picket pulse was timed by a variable delay line, and the spike pulse timing was varied by using different pulse shapes that were designed so that the low-intensity foot drive was kept the same but had a different temporal onset of the spike portion, which was varied in 100-ps time increments. The trailing edge of the main drive pulse was designed to keep the total laser energy constant.

The diagnostics that were used to measure the implosion performance include proton wedged range filters (WRFs),[20] a nuclear temporal diagnostic (NTD),[21,22] and neutron time-of-flight diagnostics comprising scintillator counters coupled to fast photomultipliers for primary and secondary neutron yield measurements.[23] The kinetic energy downshift of protons generated by the D^{3}He fusion reactions, which is a secondary-proton production reaction in D$_2$ fuel, was used to infer areal density[24,25]

$$D + D \rightarrow {}^3He + n, \tag{1}$$

followed by

$$^3He + D \rightarrow p(12.6\text{–}17.5 \text{ MeV}) + {}^4He. \tag{2}$$

The secondary protons have a considerable energy spread due to the kinetic-energy spread of ^{3}He produced in the primary reaction. The protons produced in the central hot-spot region pass through the dense and cold shell where their kinetic energy suffers a considerable downshift. Therefore the measurement of the downshifted kinetic-energy spectrum provides information about the shell areal density. By using wedges with an appropriate range of thicknesses and a CR-39 plastic detector, it is possible to make an accurate reconstruction of the proton spectrum by applying the technique discussed by Séguin et al. in Ref. 20. The lower detection limit given by the thinnest wedge section is ~4 MeV. The proton spectra were measured at four locations around the target. Areal-density measurements based on the fusion proton-spectrum downshift are routinely used at LLE.[25,26]

III. FUSION-REACTION-YIELD MEASUREMENTS OF PLASTIC-SHELL IMPLOSIONS

A series of plastic-shell implosions with D$_2$-fill pressures in the range of 9–45 atm were performed with and without SSD using low-adiabat pulse shapes without spike portion [Fig. 4(a)]. The pulse shapes were similar to that shown in Fig. 2 (dashed curve) but with a higher main drive power of ~11–13 TW. The ratio of the measured primary neutron yield to that predicted by 1D simulations using the hydrodynamic code LILAC,[27] or neutron yield-over-clean (YOC), is shown in Fig. 4(b) as a function of the calculated hot-spot convergence ratio (bottom) and fill pressure (top). The calculated hot-spot convergence ratio (CR) is defined as the
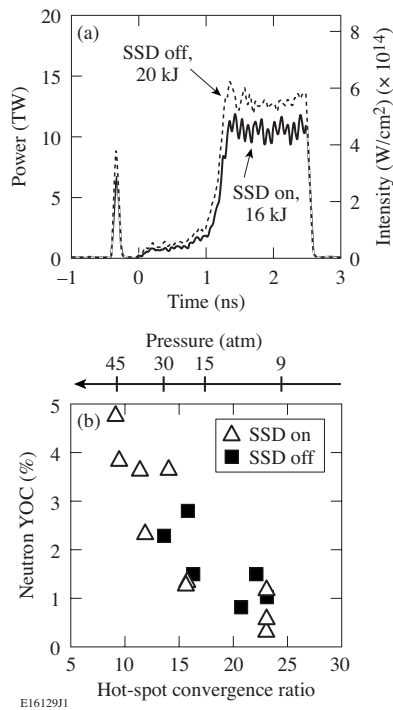
FIG. 4. (a) Low-adiabat relaxation laser pulse shapes without spike pulse. (b) Measured neutron yield over clean vs hot-spot convergence ratio (bottom) and D_2-fill pressure (top) of plastic-shell implosions. Measurement with SSD is depicted by the open triangles and without SSD by the solid square symbols.
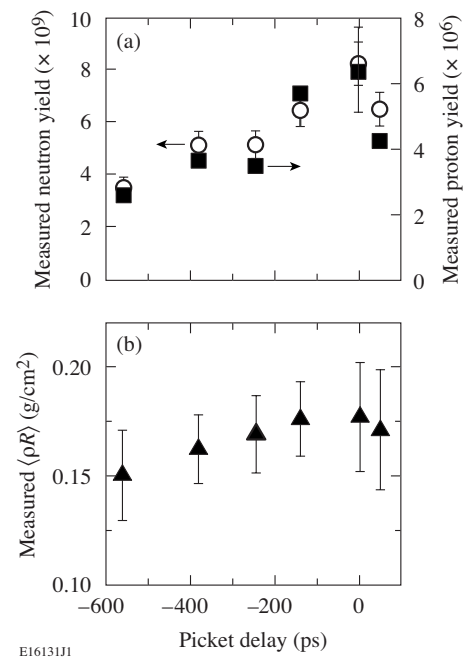

FIG. 5. (a) Measured neutron (open circles) and proton (solid squares) yields as a function of the picket-pulse timing. Zero determines the onset of the foot of the main drive and an increased negative delay shifts the picket earlier in time away from the foot. (b) Corresponding measured average areal density. The relative $\langle \rho R \rangle$ error bars are shown.

initial inner-target-shell radius divided by the minimum radius of the gas-shell interface at peak compression. The YOC is ∼4% at 45 atm and decreases with lower pressure and higher CR to ∼1%. SSD has no significant effect on the yield performance. A YOC decrease by a factor of ∼4, when CR increases from ∼9 to ∼23, indicates an increased small length mixing for smaller hot-spot radii. Large convergence ratios of the fuel and the slow assembly make plastic shells strongly RT instable during the deceleration phase, giving rise to a substantial shell-fuel mixing[28] that quenches fusion reactions and typically results in YOC of a few percent.[10] Mixing is enhanced in these low-velocity implosions because the hot spot is small relative to the target size.[29] In comparison, shock-ignition-type pulse shapes considerably improve the performance (see Fig. 7 below).

A systematic study of low-adiabat ($\alpha \approx 1.5$) plastic-shell implosions with a short picket and a high-intensity spike was performed at a constant pressure of 25 atm, a fixed laser energy of 17 kJ, and a fixed spike pulse timing of 2.8 ns as a function of picket timing (see Fig. 5). The measured neutron (open circles) and proton (solid squares) numbers are shown in Fig. 5(a) as a function of the picket-pulse delay. Zero determines the onset of the foot of the main drive and an increased delay shifts the picket earlier in time away from the foot. The neutron and proton yields increase by a factor of ∼2 from $3.5 \pm 0.4 \times 10^9$ to $8.0 \pm 0.8 \times 10^9$ and $2.6 \pm 0.5 \times 10^6$ to $6.2 \pm 1.2 \times 10^6$, respectively, when shifting from −550 ps to zero, which is the optimum picket timing. Calculated neutron and proton yields using the 1D hydrocode LILAC and a constant flux limiter of 0.06 show a similar

trend, but the predicted yield variation is not as pronounced as in the measurement. Figure 5(b) shows that the picket timing also affects the assembled average areal density ($\langle \rho R \rangle$). An ∼100-ps mistiming lowers the yield by ∼25%, which is significant compared to the neutron-yield measurement uncertainty of ∼10% and a delay by up to approximately −550 ps degrades the yield by a factor of ∼2 and $\langle \rho R \rangle$ by ∼20%. The measurement shows how shock wave timing of SW and CW affects the implosion performance of these surrogate targets, see Fig. 3. If the CW is too late, the first shock enters the fuel, prematurely compressing and heating it, while if the CW is too early, the inner target portion is placed on too high an adiabat, reducing its compressibility. For direct-drive, hot-spot ignition target designs, the CW must overtake the first shock within ±150 ps of the design specification.[30] For the surrogate CH experiments, time-zero results for both the yield and $\langle \rho R \rangle$ to the best values with $\langle \rho R \rangle = 0.18 \pm 0.02$ g/cm^2 under the experimental conditions of Fig. 5, showing that the correct timing of SW and CW has been obtained. More details on the areal-density measurements are discussed in Sec. IV.

The implosion was further optimized by studying how the timing of the SSW affects the implosion performance. This was done with different pulse shapes that were designed to have the same low-intensity foot and plateau, but different spike pulse timing. Figure 6(a) shows an overview of the neutron-yield measurements. The dot-data point represents a measurement for a pulse shape without a high-intensity spike, yielding $1.8 \pm 0.2 \times 10^9$ neutrons with 19.4-kJ laser energy. In comparison, a spike pulse with a 2.8-ns delay and slightly less laser energy (18.6 kJ) results in four times more neutrons ($8.0 \pm 0.8 \times 10^9$, upper triangle). The proton yield
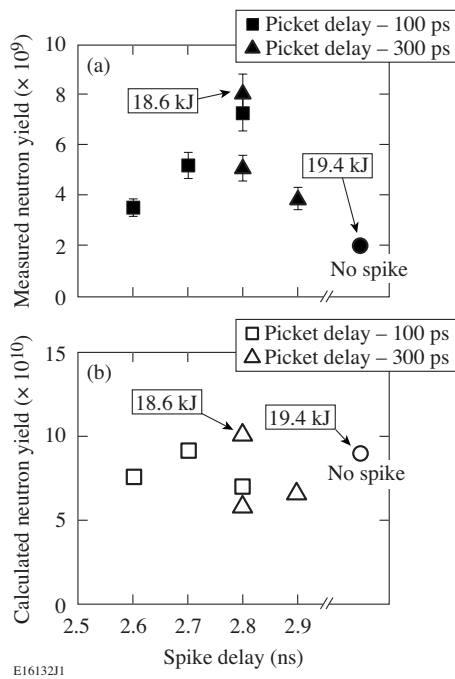
FIG. 6. (a) Measured neutron yield as a function of the onset of the spike pulse, for two different picket-pulse delays. The targets were filled with 25 atm of D_2. The pulse without spike (dot) used a 300-ps picket delay. (b) Calculated neutron yield vs spike pulse delay.

FIG. 7. The neutron YOC vs 1D calculated hot-spot convergence ratio. The YOC is close to 10% for a hot-spot convergence of up to 30.

increases by a factor of ~5 from $1.3 \pm 0.3 \times 10^6$ to $6.2 \pm 1.2 \times 10^6$. All other data points were measured with ~17-kJ laser energy, which explains why the second triangle at 2.8 ns is lower. The triangles represent the measurement for a picket delay of −300 ps, and the squares are a series with −100-ps picket delay. Figure 5(a) shows that a shorter picket delay results in an improved yield, which is consistent with the fact that the square data points in Fig. 6(a) are slightly higher than the triangles. The measurement in Fig. 6(a) demonstrates an optimum timing of the spike pulse delay at 2.8 ns. A mistiming by 100 ps significantly affects the yield performance. One-dimensional hydrodynamic simulations using the code LILAC do not predict a maximum in neutron yield at 2.8 ns and show very little sensitivity of the fusion product yield on SSW timing [see Fig. 6(b)]. The calculated 1D yield for the SSW implosion with 18.6 kJ (upper triangle at 2.8 ns) is only slightly higher than a comparable implosion without SSW and 19.4 kJ of laser energy. Calculations for exactly the same laser energy predict ~30% yield enhancement by the SSW, which is much lower than measured. As mentioned before, the SSW energy coupling into the hot spot is optimal for thick-shell targets because the ignitor shock strength increases significantly when traveling through the converging shell. Compared to an ignition design with a target shell thickness of ~350 μm (Ref. 5), the present targets (40-μm CH, ~100-μm cryo) are thin-shell targets, which explains why the simulated enhancement is only marginal. It is not yet clear why the targets perform much better than predicted, but there are several possible explanations. Plastic shells with low-pressure fills are inherently RT instable during the deceleration phase, giving rise to substantial shell-fuel mixing that quenches fusion reactions,
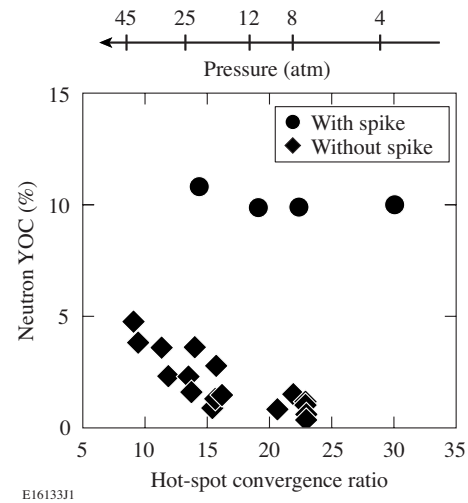
which is believed to be the main cause for the YOCs in the percent range. The experiments presented here suggest that for optimal SSW timing, the mixing processes are mitigated, which might be caused by the impulse acceleration by the SSW that shortens the time period for the instability growth or by the steepening of the density profile at the inner shell surface. Another possibility, which is not very likely, would be that the hot-spot heat-transport losses are not modeled correctly and that the temperature increase produced by the SSW is larger than predicted leading to the higher yield. Multidimensional hydrodynamic simulations have been started to study this effect in more detail.

The implosion performance was studied with the optimized spike pulse shape for various shell-fill pressures between 4 and 25 atm. Figure 7 compares the YOC versus CR for implosions with optimized spike pulse shape (dots) and various pulse forms without spike pulse (diamonds), including the data from Fig. 4(b). The implosions without spike pulse were not optimized with respect to shock wave timing. The experiments demonstrate that YOC close to 10% has been obtained for plastic-shell, $\alpha=1.5-1.9$, low-adiabat implosions and CR of up to 30, indicating an improved stability with shock-ignition-type pulse shapes.

IV. AREAL-DENSITY ANALYSIS OF PLASTIC-SHELL IMPLOSIONS

Figure 8 shows the measured proton spectrum, which is the average of four individual proton spectra taken from different lines of sights, for an 8.3-atm, D_2-fill implosion with a laser energy of 18 kJ without SSD. All of the measurements described in this section were performed without SSD. A mean downshift of 6.38 ± 0.13 MeV was measured where the error represents the standard deviation over the four measurements. Following Ref. 24, an areal density averaged over the proton spectral distribution of $\langle \rho R \rangle = 0.204 \pm 0.003$ g/cm^2 is inferred where the uncertainty represents the standard deviation of $\langle \rho R \rangle$ from the four measurements. No significant effect of SSD smoothing on ρR was found for relaxation-type low-adiabat implosions,[10] and the
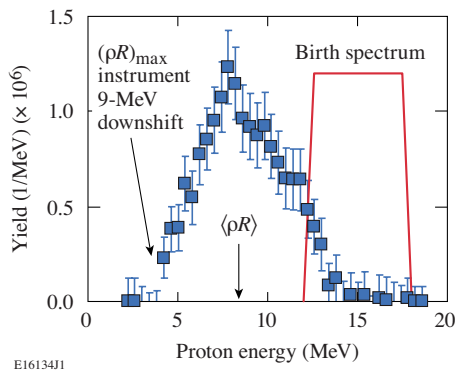
FIG. 8. (Color online) Measured proton spectra for shot 48674, which is the average of four spectra taken from different directions. The 8.3-atm-D_2-filled CH shell was imploded with 18.0 kJ without SSD. The average areal density was measured with $\langle\rho R\rangle = 0.204 \pm 0.014$ g/cm^2, and the measured maximum areal density of 0.3 g/cm^2 is restricted by the detection limit of the instrument.

FIG. 9. (Color online) $\langle\rho R\rangle$ vs CR for 2.8-ns spike-delay pulse implosions (optimized pulse shape, solid triangle; picket mistimed, open triangles) and no-spike pulse-shape implosions (open squares). The relative $\langle\rho R\rangle$ error bars are shown.

small standard deviation of the ρR measurement indicates high shell stability. Notice that the lower limit of the detector given by the thickness of the Al wedges[20] is at a proton energy of 4 MeV, which appears as a cutoff in the measured spectrum. The protons need to be downshifted by ~9 MeV to reach the cutoff that corresponds to a ρR value of ~0.3 g/cm^2. Therefore, the proton spectrum indicates that areal densities even higher than 0.3 g/cm^2 were experimentally realized. Calculations with the 1D code LILAC (Ref. 27) using a constant flux limiter of 0.06 predict, for shot 48674, $(\rho R)_{max} = 0.345$ g/cm^2 and with a time-dependant flux limiter (Refs. 31 and 32) $(\rho R)_{max} = 0.331$ g/cm^2. The time-dependant flux-limiter calculations model the nonlocal heat transport by introducing an effective temporal varying flux limiter.[32] For the ρR inference a fusion-reaction-rate-averaged density of 110 g/cm^3 and a temperature of 0.1 keV were taken from simulations. The inferred ρR value depends slightly on the density. A density variation of ± 50 g/cm^3 changes the areal density by $\sim \pm 0.01$ g/cm^2. The temperature dependence is negligible. The absolute calibration uncertainty of the WRF is ± 0.4 MeV for the mean value of the proton spectral distribution corresponding to ± 0.01 g/cm^2. Taking the statistical fluctuation, the density variation, and the calibration uncertainty into account, an absolute measurement error of $\sim \pm 0.014$ g/cm^2 is estimated, leading to $\langle\rho R\rangle = 0.204 \pm 0.014$ g/cm^2.

Areal-density measurements were performed for various fill pressures corresponding to various hot-spot convergence ratios. Figure 9 shows that implosions with optimized spike pulse shapes (solid triangles) achieve the highest $\langle\rho R\rangle$ values that have a tendency to increase with CR from ~15 to ~25. The data point at CR ~30 falls below the scaling indicating that for large CR the $\langle\rho R\rangle$ measurement is affected by the instrumental cutoff and by the sampling over the $\langle\rho R\rangle$-time evolution (see below). The solid line is a linear fit through the first three solid triangle data points. In contrast, lower $\langle\rho R\rangle$ values are measured for a mistimed picket (open triangles) and the lowest $\langle\rho R\rangle$ values are observed without SSW (squares), showing also a larger data scattering. Figures 7 and 9 reveal that optimum timed shock-ignition pulse-
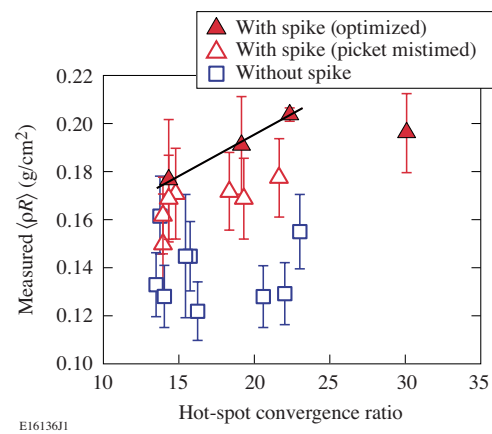
shape implosions show an improved performance with higher $\langle\rho R\rangle$ and suggest less instability growth.

Figure 10(a) shows all of the measured SSW implosion $\langle\rho R\rangle$ data versus the 1D prediction with a time-dependent flux limiter. To relate the measured $\langle\rho R\rangle$ obtained from the mean of the proton spectrum to the 1D calculation, the predicted ρR evolution is averaged over a time window in which the fusion products are generated and weighted according to the production rate.[33] The simulations in Fig. 10(b) show that

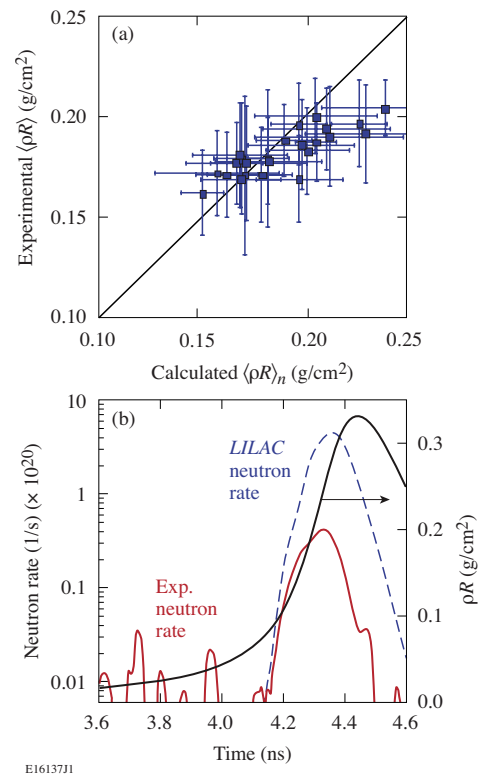
FIG. 10. (Color online) (a) Measured spike-pulse implosion $\langle\rho R\rangle$ vs LILAC calculated neutron-rate-averaged $\langle\rho R\rangle_n$ and (b) comparison of measured neutron rate (solid curve), 1D predicted neutron rate (dashed curve), and predicted ρR evolution (solid curve) for shot 48674 (proton spectrum in Fig. 8). The absolute measurement $\langle\rho R\rangle$ uncertainties are shown in (a).

the ρR (solid black curve) increases during neutron production and that the fusion reactions are quenched near the time of a peak areal density of 0.33 g/cm^2. The measured neutron rate (solid red curve) is lower and truncated compared to the 1D simulated fusion rate (dashed), probably caused by shell-fuel mixing. Mixing is a time-dependant process that is small in the initial phase of ρR buildup and then grows during the deceleration, leaving a clean hot-spot radius equal to the so-called free-fall line.[34] The corresponding time-integrated proton spectrum is shown in Fig. 8; each point of the spectrum corresponds to a different downshift and, therefore, to a different ρR. The energy downshift of the low-energy tail of the spectrum represents a measure of the peak ρR during the neutron production, which was limited by the instrument indicating peak ρR exceeding 0.3 g/cm^2, in agreement with the simulations. The temporal shape of the neutron-production rate is close to the secondary proton-production rate[26] and is used to calculate the neutron-rate-averaged $\langle \rho R \rangle_n$ [Fig. 10(a)]. The experimental error of the absolute timing of NTD (Ref. 22) is ~50 ps and, considering that the neutron-production duration is typically less than 300 ps, the calculated $\langle \rho R \rangle_n$ values are very sensitive to the timing of the measured neutron rate. The timing error of the measured rate was taken into account for these calculations, leading to the uncertainties in the calculated $\langle \rho R \rangle_n$ shown as *x*-error bars in Fig. 10(a). Figure 10 shows that the fuel assembly is close to the burn-weighted 1D predictions of the code LILAC with measured ρR values achieving larger than 90% of the 1D prediction. The slight deviation at high compression is partially due to the instrumental cutoff resulting in a slightly lower $\langle \rho R \rangle$ reading.

V. INITIAL SPIKE-PULSE CRYOGENIC-SHELL IMPLOSIONS

Initial shock-spike implosions with cryogenic D$_2$ and DT targets [Fig. 1(b)] were performed using spike-pulse shapes similar to that shown in Fig. 2 with a total laser energy of 16.0 kJ for the D$_2$ target and 17.9 kJ for the DT target. In both cases SSD was used. High-quality targets with ice-layer nonuniformities of $\sigma_{rms} = 1.5$ μm (D$_2$) and 0.9 μm (DT) were imploded. The D$_2$ target implosion suffered from a large 49 ± 3-μm offset of the capsule center from the target chamber center, which caused a significant drive asymmetry. A low-mode ρR modulation was measured with the higher areal density toward the higher-intensity drive side. By averaging the four lines of sight, an areal density of $\langle \rho R \rangle = 0.18 \pm 0.05$ g/cm^2 was measured, which is compared to a calculated value of 0.20 g/cm^2 (time-dependent flux limiter)[32] taking the measured fusion-reaction history into account. Therefore, the assembled fuel reaches ~90% of the 1D prediction. The neutron yield is ~5% of the 1D prediction. A similar D$_2$ cryogenic-target implosion using a similar waveform but without a spike pulse and with a better target offset of 19 ± 3 μm yielded a slightly higher YOC of ~7% and $\langle \rho R \rangle = 0.20 \pm 0.02$ g/cm^2 (Ref. 35). Table I compares the implosion performance of cryogenic targets using low-adiabat picket-pulse shapes with and without a high-intensity spike at the end of the drive pulse. No measured ρR data are

TABLE I. A comparison of the implosion performance of cryogenic targets using low-adiabat picket pulse shapes with and without a high-intensity spike at the end of the drive pulse.

Shot No.	47206	48386	48304	48734
Target	D$_2$	D$_2$	DT	DT
Ice layer σ (μm)	2.4	1.5	0.7	0.9
Target offset (μm)	19 ± 3	49 ± 3	No data	10 ± 5
Spike pulse	No	Yes	No	Yes
E_{laser} (kJ)	16.5	16.0	19.3	17.9
Adiabat	1.8	2.0	2.0	2.0
$\langle \rho R \rangle_{exp}$ (g/cm^2)	0.201 ± 0.021	0.182 ± 0.046	No data	No data
$\langle \rho R \rangle_{LILAC}$ (g/cm^2)	0.216	0.204	0.186	0.194
T_{ion} (keV) (Expt)	2.1 ± 0.5	1.8 ± 0.5	2.5 ± 0.5	1.9 ± 0.5
T_{ion} (keV) (LILAC)	2.0	1.9	2.3	2.3
Y_n	7.70×10^9	3.40×10^9	1.60×10^{12}	1.43×10^{12}
(YOC)	7.3%	5.3%	9.8%	12.3%

available for the DT implosions because the WRF diagnostic is compromised by the large neutron influx. DT target shot 48734 (with a late spike pulse) had very good ice-layer quality and small target offset resulting in YOC of ~12%, while a comparable shot without spike pulse (48304) gave a YOC of ~10%. Due to a diagnostic error, no target-offset data are available for shot 48304. The first few shock-ignition cryo implosions on OMEGA were among the best performing (in terms of yield and ρR) but did not yet exceed the performance of standard pulse shapes. This is likely due to a non-optimal pulse shape when SSD was employed. The SSD bandwidth broadened the spike pulse sufficiently so that LILAC simulations do not show a SSW. The spike pulse rise time without SSD in the plastic-shell implosions is about twice as fast and generates a significant SSW. Further experimental studies will assess the implosion performance of cryogenic targets without SSD and working toward an improved pulse shape with SSD, which will then allow a strong enough shock with the late spike pulse to be generated.

Parametric plasma instabilities are of concern in an ignition target design[5] with spike-pulse intensities in the range of 10^{15}–10^{16} W/cm^2 and ~150-ps FWHM pulse. The instabilities increase the back-reflection of laser light from the target and therefore lower the coupling efficiency into the capsule, while an increased fraction of the coupled energy will be transferred into suprathermal electrons, which are a potential source of preheat. No measurable amount of stimulated Raman and Brillouin backscatter is detected in the above-discussed cryogenic implosions having nominal laser peak intensities of $\sim 8 \times 10^{14}$ W/cm^2. The actual intensity at the critical-density surface is a factor of ~2 higher when the target compression is taken into account. There is a measurable amount of hard x-ray yield above ~50 keV due to fast electrons produced by the two-plasmon-decay (TPD) instability. Since $\langle \rho R \rangle$ reaches ~90% of the 1D prediction, there is no significant degradation of the implosion due to preheat. There are no parametric-instability measurements for shock-ignition-target relevant conditions available (spherical cryogenic target, long density scale length, and intensities above 2×10^{15} W/cm^2). However, measurements of parametric in-

stabilities for indirect-drive-relevant ignition-plasma conditions with millimeter-density scale length and 15% critical-density targets report a backscatter of the order of a few percent to 10% at 5×10^{15}-W/cm² (Ref. 36). The density scale lengths in shock-ignition targets are shorter and for similar laser intensities the backscatter is expected to be of the order of ~10% or less. Parametric instability and fast-electron-generation scaling measurements at direct-drive-ignition-relevant intensities and long density scale lengths in warm surrogate targets show that the TPD-generated preheat starts to saturate at intensities above $\sim 1 \times 10^{15}$ W/cm² (Ref. 37). Moderate-energy fast electrons (~100 keV) generated by the late high-intensity spike might even be beneficial for the shock-ignition concept. The effect of preheating was studied in marginal igniting, 350-μm-thick massive shells with the 1D LILAC code using a multigroup diffusion model for the fast-electron transport and a Maxwellian hot-electron-energy distribution of 150-keV characteristic energy.[5] There is considerable compression at the time when the fast electrons are generated with $\langle \rho R \rangle \approx 70$ mg/cm², compared to a 17-mg/cm² stopping range of a 100-keV electron in the cryogenic DT shell. The majority of the fast electrons are stopped in the outer layers of the shell and pose no threat of the implosion performance being compromised by preheat. Moderate-energy fast electrons actually increase the strength of the SSW, therefore widening the shock-launching ignition window.[5]

VI. SUMMARY AND CONCLUSIONS

Fuel assembly that is relevant for the shock-ignition ICF concept has been experimentally studied for the first time. The experiments were performed on the OMEGA Laser Facility at the University of Rochester's Laboratory for Laser Energetics using shock-ignition laser pulse shapes and warm plastic surrogate and cryogenic targets. Systematic studies of low-adiabat ($\alpha \approx 1.5$) implosions with a short picket and a high-intensity spike were performed. It was demonstrated that the fuel assembly with warm plastic targets is close to 1D simulation predictions with neutron-rate-averaged areal densities exceeding ~0.2 g/cm² and maximum ρR above ~0.3 g/cm², which are significantly higher than without the spike pulse. Implosions of D₂-filled, 40-μm-thick plastic shells were optimized by measuring the performance as a function of the timing of the picket and spike pulses. The spike-shock-generated implosion produces a factor of ~4-enhanced neutron yield compared to a laser pulse shape without intensity spike for 25-atm fill pressure and the same laser energy. For an optimized spike-pulse shape with respect to shock wave timing, the measured neutron yields are ~10% of the yields calculated by 1D simulations (YOC) for fill pressures down to 4 atm, while the YOC without a spike pulse (not optimized) is less than 1% for pressures below 9 atm. These are the highest YOCs reported so far for $\alpha \approx 1.5$ implosions of warm plastic shells and a hot-spot convergence ratio of ~30. Plastic shells with low fill pressures are inherently RT-instable during the deceleration phase, giving rise to a substantial shell-fuel mixing that quenches fusion reactions, which is not described by 1D simulations.

The measurements have shown that the shock-ignition concept is very promising by achieving higher compression and better stability than comparable low-adiabat, relaxation-picket plastic-shell implosions without a spike pulse. Initial experiments with cryogenic D₂ and DT targets and $\alpha = 2$, spike and no-spike pulse shapes were performed, showing close to 1D performance and a neutron YOC of ~12%.

[1] J. Nuckolls, L. Wood, A. Thiessen, and G. Zimmerman, Nature (London) **239**, 139 (1972).

[2] J. D. Lindl, *Inertial Confinement Fusion: The Quest for Ignition and Energy Gain Using Indirect Drive* (Springer-Verlag, New York, 1998), p. 4.

[3] S. Atzeni and J. Meyer-ter-Vehn, *The Physics of Inertial Fusion: Beam Plasma Interaction, Hydrodynamics, Hot Dense Matter*, International Series of Monographs on Physics (Clarendon, Oxford, 2004), p. 52.

[4] R. Betti, C. D. Zhou, K. S. Anderson, L. J. Perkins, W. Theobald, and A. A. Solodov, Phys. Rev. Lett. **98**, 155001 (2007).

[5] R. Betti, W. Theobald, C. D. Zhou, K. S. Anderson, P. W. McKenty, D. Shvarts, and C. Stoeckl, "Shock ignition of thermonuclear fuel with high areal densities," presented at the Fifth International Conference on Inertial Fusion Sciences and Applications (IFSA 2007), Kobe, Japan, 9–14 September 2007, J. Phys.: Conf. Ser. (submitted).

[6] M. C. Herrmann, M. Tabak, and J. D. Lindl, Phys. Plasmas **8**, 2296 (2001).

[7] M. Tabak, J. Hammer, M. E. Glinsky, W. L. Kruer, S. C. Wilks, J. Woodworth, E. M. Campbell, M. D. Perry, and R. J. Mason, Phys. Plasmas **1**, 1626 (1994).

[8] M. Murakami and H. Nagatomo, Nucl. Instrum. Methods Phys. Res. A **544**, 67 (2005).

[9] R. Betti and C. Zhou, Phys. Plasmas **12**, 110702 (2005); R. Betti, K. Anderson, T. R. Boehly, T. J. B. Collins, R. S. Craxton, J. A. Delettrez, D. H. Edgell, R. Epstein, V. Yu. Glebov, V. N. Goncharov, D. R. Harding, R. L. Keck, J. H. Kelly, J. P. Knauer, S. J. Loucks, J. A. Marozas, F. J. Marshall, A. V. Maximov, D. N. Maywar, R. L. McCrory, P. W. McKenty, D. D. Meyerhofer, J. Myatt, P. B. Radha, S. P. Regan, C. Ren, T. C. Sangster, W. Seka, S. Skupsky, A. A. Solodov, V. A. Smalyuk, J. M. Soures, C. Stoeckl, W. Theobald, B. Yaakobi, C. Zhou, J. D. Zuegel, J. A. Frenje, C. K. Li, R. D. Petrasso, and F. H. Séguin, Plasma Phys. Controlled Fusion **48**, B153 (2006).

[10] C. D. Zhou, W. Theobald, R. Betti, P. B. Radha, V. A. Smalyuk, D. Shvarts, V. Yu. Glebov, C. Stoeckl, K. S. Anderson, D. D. Meyerhofer, T. C. Sangster, C. K. Li, R. D. Petrasso, J. A. Frenje, and F. H. Séguin, Phys. Rev. Lett. **98**, 025004 (2006).

[11] T. R. Boehly, D. L. Brown, R. S. Craxton, R. L. Keck, J. P. Knauer, J. H. Kelly, T. J. Kessler, S. A. Kumpan, S. J. Loucks, S. A. Letzring, F. J. Marshall, R. L. McCrory, S. F. B. Morse, W. Seka, J. M. Soures, and C. P. Verdon, Opt. Commun. **133**, 495 (1997).

[12] C. Stoeckl, C. Chiritescu, J. A. Delettrez, R. Epstein, V. Yu. Glebov, D. R. Harding, R. L. Keck, S. J. Loucks, L. D. Lund, R. L. McCrory, P. W. McKenty, F. J. Marshall, D. D. Meyerhofer, S. F. B. Morse, S. P. Regan, P. B. Radha, S. Roberts, T. C. Sangster, W. Seka, S. Skupsky, V. A. Smalyuk, C. Sorce, J. M. Soures, R. P. J. Town, J. A. Frenje, C. K. Li, R. D. Petrasso, F. H. Séguin, K. Fletcher, S. Padalino, C. Freeman, N. Izumi, R. Lerche, and T. W. Phillips, Phys. Plasmas **9**, 2195 (2002).

[13] T. C. Sangster, J. A. Delettrez, R. Epstein, V. Yu. Glebov, V. N. Goncharov, D. R. Harding, J. P. Knauer, R. L. Keck, J. D. Kilkenny, S. J. Loucks, L. D. Lund, R. L. McCrory, P. W. McKenty, F. J. Marshall, D. D. Meyerhofer, S. F. B. Morse, S. P. Regan, P. B. Radha, S. Roberts, W. Seka, S. Skupsky, V. A. Smalyuk, C. Sorce, J. M. Soures, C. Stoeckl, K. Thorp,

J. A. Frenje, C. K. Li, R. D. Petrasso, F. H. Séguin, K. A. Fletcher, S. Padalino, C. Freeman, N. Izumi, J. A. Koch, R. A. Lerche, M. J. Moran, T. W. Phillips, and G. J. Schmid, Phys. Plasmas **10**, 1937 (2003).

[14] T. C. Sangster, R. Betti, R. S. Craxton, J. A. Delettrez, D. H. Edgell, L. M. Elasky, V. Yu. Glebov, V. N. Goncharov, D. R. Harding, D. Jacobs-Perkins, R. Janezic, R. L. Keck, J. P. Knauer, S. J. Loucks, L. D. Lund, F. J. Marshall, R. L. McCrory, P. W. McKenty, D. D. Meyerhofer, P. B. Radha, S. P. Regan, W. Seka, W. T. Shmayda, S. Skupsky, V. A. Smalyuk, J. M. Soures, C. Stoeckl, B. Yaakobi, J. A. Frenje, C. K. Li, R. D. Petrasso, F. H. Séguin, J. D. Moody, J. A. Atherton, B. D. McGowan, J. D. Kilkenny, T. P. Bernat, and D. S. Montgomery, Phys. Plasmas **14**, 058101 (2007).

[15] T. R. Boehly, V. A. Smalyuk, D. D. Meyerhofer, J. P. Knauer, D. K. Bradley, R. S. Craxton, M. J. Guardalben, S. Skupsky, and T. J. Kessler, J. Appl. Phys. **85**, 3444 (1999).

[16] Y. Lin, T. J. Kessler, and G. N. Lawrence, Opt. Lett. **21**, 1703 (1996).

[17] S. Skupsky, R. W. Short, T. Kessler, R. S. Craxton, S. Letzring, and J. M. Soures, J. Appl. Phys. **66**, 3456 (1989).

[18] K. Anderson and R. Betti, Phys. Plasmas **11**, 5 (2004).

[19] J. P. Knauer, K. Anderson, R. Betti, T. J. B. Collins, V. N. Goncharov, P. W. McKenty, D. D. Meyerhofer, P. B. Radha, S. P. Regan, T. C. Sangster, V. A. Smalyuk, J. A. Frenje, C. K. Li, R. D. Petrasso, and F. H. Séguin, Phys. Plasmas **12**, 056306 (2005).

[20] F. H. Séguin, J. A. Frenje, C. K. Li, D. G. Hicks, S. Kurebayashi, J. R. Rygg, B.-E. Schwartz, R. D. Petrasso, S. Roberts, J. M. Soures, D. D. Meyerhofer, T. C. Sangster, J. P. Knauer, C. Sorce, V. Yu. Glebov, C. Stoeckl, T. W. Phillips, R. J. Leeper, K. Fletcher, and S. Padalino, Rev. Sci. Instrum. **74**, 975 (2003).

[21] R. A. Lerche, D. W. Phillion, and G. L. Tietbohl, Rev. Sci. Instrum. **66**, 933 (1995).

[22] C. Stoeckl, V. Yu. Glebov, S. Roberts, T. C. Sangster, R. A. Lerche, R. L. Griffith, and C. Sorce, Rev. Sci. Instrum. **74**, 1713 (2003).

[23] V. Yu. Glebov, D. D. Meyerhofer, C. Stoeckl, and J. D. Zuegel, Rev. Sci. Instrum. **72**, 824 (2001).

[24] C. K. Li, D. G. Hicks, F. H. Séguin, J. A. Frenje, R. D. Petrasso, J. M. Soures, P. B. Radha, V. Yu. Glebov, C. Stoeckl, D. R. Harding, J. P. Knauer, R. L. Kremens, F. J. Marshall, D. D. Meyerhofer, S. Skupsky, S. Roberts, C. Sorce, T. C. Sangster, T. W. Phillips, M. D. Cable, and R. J. Leeper, Phys. Plasmas **7**, 2578 (2000).

[25] R. D. Petrasso, J. A. Frenje, C. K. Li, F. H. Séguin, J. R. Rygg, B. E. Schwartz, S. Kurebayashi, P. B. Radha, C. Stoeckl, J. M. Soures, J. Delettrez, V. Yu. Glebov, D. D. Meyerhofer, and T. C. Sangster, Phys. Rev. Lett. **90**, 095002 (2003).

[26] V. A. Smalyuk, P. B. Radha, J. A. Delettrez, V. Yu. Glebov, V. N. Gon-charov, D. D. Meyerhofer, S. P. Regan, S. Roberts, T. C. Sangster, J. M. Soures, C. Stoeckl, J. A. Frenje, C. K. Li, R. D. Petrasso, and F. H. Séguin, Phys. Rev. Lett. **90**, 135002 (2003).

[27] J. Delettrez, R. Epstein, M. C. Richardson, P. A. Jaanimagi, and B. L. Henke, Phys. Rev. A **36**, 3926 (1987); M. C. Richardson, P. W. McKenty, F. J. Marshall, C. P. Verdon, J. M. Soures, R. L. McCrory, O. Barnouin, R. S. Craxton, J. Delettrez, R. L. Hutchinson, P. A. Jaanimagi, R. Keck, T. Kessler, H. Kim, S. A. Letzring, D. M. Roback, W. Seka, S. Skupsky, B. Yaakobi, S. M. Lane, and S. Prussin, in *Laser Interaction and Related Plasma Phenomena*, edited by H. Hora and G. H. Miley (Plenum, New York, 1986), Vol. 7, p. 421.

[28] P. B. Radha, T. J. B. Collins, J. A. Delettrez, Y. Elbaz, R. Epstein, V. Yu. Glebov, V. N. Goncharov, R. L. Keck, J. P. Knauer, J. A. Marozas, F. J. Marshall, R. L. McCrory, P. W. McKenty, D. D. Meyerhofer, S. P. Regan, T. C. Sangster, W. Seka, D. Shvarts, S. Skupsky, Y. Srebro, and C. Stoeckl, Phys. Plasmas **12**, 056307 (2005).

[29] C. D. Zhou and R. Betti, Phys. Plasmas **14**, 072703 (2007).

[30] T. R. Boehly, E. Vianello, J. E. Miller, R. S. Craxton, T. J. B. Collins, V. N. Goncharov, I. V. Igumenshchev, D. D. Meyerhofer, D. G. Hicks, P. M. Celliers, and G. W. Collins, Phys. Plasmas **13**, 056303 (2006).

[31] A. Sunahara, J. A. Delettrez, C. Stoeckl, R. W. Short, and S. Skupsky, Phys. Rev. Lett. **91**, 095003 (2003).

[32] V. N. Goncharov, O. V. Gotchev, E. Vianello, T. R. Boehly, J. P. Knauer, P. W. McKenty, P. B. Radha, S. P. Regan, T. C. Sangster, S. Skupsky, V. A. Smalyuk, R. Betti, R. L. McCrory, D. D. Meyerhofer, and C. Cherfils-Clérouin, Phys. Plasmas **13**, 012702 (2006).

[33] P. B. Radha, V. Yu. Glebov, V. N. Goncharov, D. D. Meyerhofer, T. C. Sangster, S. Skupsky, J. A. Frenje, and R. D. Petrasso, Bull. Am. Phys. Soc. **51**, 104 (2006).

[34] P. D. Roberts, S. J. Rose, P. C. Thompson, and R. J. Wright, J. Phys. D **13**, 1957 (1980).

[35] T. C. Sangster, V. N. Goncharov, P. B. Radha, V. A. Smalyuk, R. Betti, R. S. Craxton, J. A. Delettrez, D. H. Edgell, V. Yu. Glebov, D. R. Harding, D. Jacobs-Perkins, J. P. Knauer, F. J. Marshall, R. L. McCrory, P. W. McKenty, D. D. Meyerhofer, S. P. Regan, W. Seka, S. Skupsky, J. M. Soures, C. Stoeckl, B. Yaakobi, D. Shvarts, J. A. Frenje, C. K. Li, R. D. Petrasso, and F. H. Séguin, "High-areal-density fuel assembly in direct-drive cryogenic implosions," Phys. Rev. Lett. (submitted).

[36] J. P. Moody, B. J. MacGowan, J. E. Rothberg, R. L. Berger, L. Divol, S. H. Glenzer, R. K. Kirkwood, E. A. Williams, and P. E. Young, Phys. Rev. Lett. **86**, 2810 (2001).

[37] C. Stoeckl, R. E. Bahr, B. Yaakobi, W. Seka, S. P. Regan, R. S. Craxton, J. A. Delettrez, R. W. Short, J. Myatt, A. V. Maximov, and H. Baldis, Phys. Rev. Lett. **90**, 235002 (2003).